Volume 19 | Number 42 | 14 November 2017 | Pages 6217–6392

CrystEngComm

rsc.li/crystengcomm

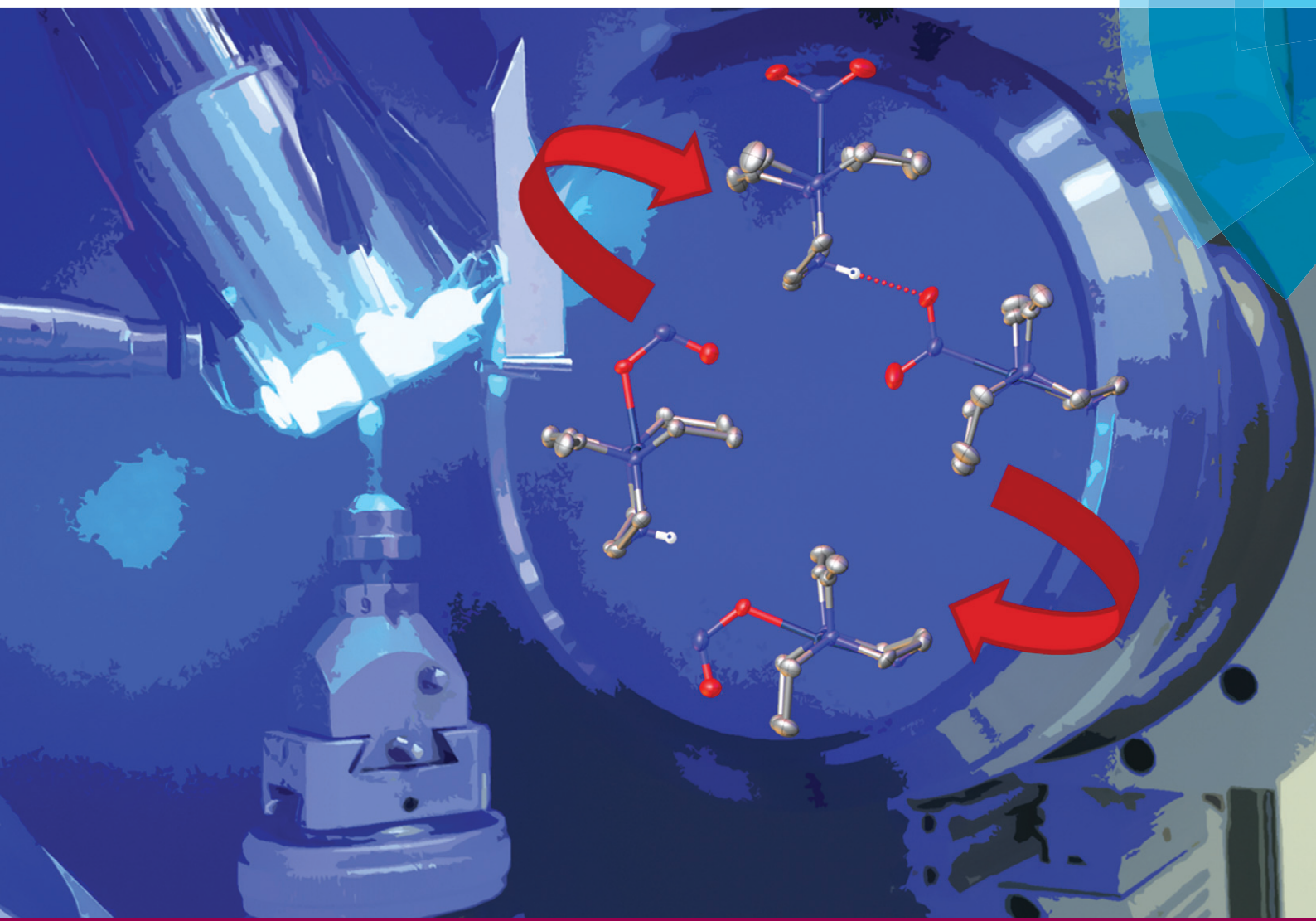

This week's cover: our 10,000th article!

ROYAL SOCIETY OF CHEMISTRY

PAPER
Lauren E. Hatcher and Paul R. Raithby
The impact of hydrogen bonding on 100% photo-switching in solid-state nitro–nitrito linkage isomers

CrystEngComm

PAPER

View Article Online
View Journal | View Issue

Cite this: *CrystEngComm*, 2017, **19**, 6297

The impact of hydrogen bonding on 100% photo-switching in solid-state nitro–nitrito linkage isomers†

Lauren E. Hatcher * and Paul R. Raithby

Received 25th July 2017,
Accepted 6th September 2017

DOI: 10.1039/c7ce01366c

rsc.li/crystengcomm

Two crystal systems: [Pd(Et_4dien)(NO_2)]OTf [**1**] and [Pt(Et_4dien)(NO_2)]OTf [**2**] (Et_4dien = *N*,*N*,*N*′,*N*′-tetraethyldiethylene-triamine, OTf = trifluoromethanesulfonate) are investigated by steady-state photo-crystallographic methods. Both structures contain intermolecular hydrogen bonds to the ground state nitro-(η^1-NO_2) isomer, which are previously shown to limit the achievable level of nitro → nitrito photo-conversion. Irradiation at 100 K induces a mixture of *endo*-ONO and *exo*-ONO isomers in **1** and **2**, with overall incomplete photo-activation. In contrast, irradiation at higher temperatures leads to much higher conversion, with 100% excitation in **1** at 150 K. The results show that the detrimental effects of hydrogen bonding on the photo-reaction are overcome at higher temperature, adding a new dimension of control to the isomerisation process.

Introduction

Solid-state photo-switchable systems, which can be reversibly shuttled between two distinct structural forms upon irradiation, are important in the search for new functional materials that can exploit the earth's most abundant clean energy source: the sun. The majority of commercially available photo-switches, for example, those exploited for photo-voltaic applications, are hampered by problems such as low photo-conversion and efficiency levels. As such, there is a need to develop methods to address these issues and ultimately to design new systems capable of high levels of photo-conversion in the solid-state.

For many decades it has been known that organometallic systems containing ambidentate ligands exist as one of several, structurally distinct linkage isomers.[1] Photo-switching between linkage isomers can be achieved in both solution and the solid-state, with irradiation of the solid leading to the production of a metastable state (MS) isomer below some critical temperature.[2] *In situ* photocrystallographic studies have to-date revealed the structures of various MS linkage isomers, including nitrosyl,[3,4] nitrite,[5–8] sulfur dioxide,[9–11] and di-nitrogen[12] systems.

Early photocrystallographic studies involving metastable linkage isomers were limited by low levels of photo-activation in the single-crystal.[11,13] However, in 2009 the first system to undergo 100% photo-switching between a ground state (GS) nitro-(η^1-NO_2) and a MS *endo*-nitrito-(η^1-ONO) isomer was reported.[7] Since then, we have reported a number of metal–nitrite systems capable of achieving very high levels of photo-induced linkage isomer conversion, designed on the basis of a simple crystal engineering principle. These systems include large, sterically-demanding ancillary fragments in the crystalline array, which are all photo-inert. These static, bulky components can then dominate the crystal packing and define a suitable "reaction cavity" around the potentially isomerisable nitrite group.[14,15] Photo-switching can then proceed to a high level within this cavity, without imparting undue strain to the rest of the crystalline array that may otherwise inhibit high conversion.

The successful implementation of this simple crystal engineering principle highlights the important influence that the surrounding crystalline environment has on the photo-switching process. Each molecule in a crystal is involved in a complicated array of intermolecular interactions, which have the potential to both assist and hinder linkage isomerism. In particular, strong-to-moderate intermolecular hydrogen bonds, involving the nitro-(η^1-NO_2) group in the ground state (GS), are shown to have a detrimental effect on the maximum level of photo-conversion that can be achieved. An example is [Ni(MeDPT)(NO_2)$_2$], which contains two, crystallographically distinct nitro-(η^1-NO_2) environments in its GS structure.[16] One NO_2 group participates in no significant hydrogen bonding and is found to reach 89% photo-activation in the excited state (ES). By contrast, a conversion level of just 32% is achieved at the second NO_2 position, which is bound by

Department of Chemistry, University of Bath, Bath, BA2 7AY, UK.
E-mail: l.e.hatcher@bath.ac.uk

† Electronic supplementary information (ESI) available. CCDC 1564437–1564451 (**1**) and 1564462–1564480 (**2**) contain the crystallographic data for this paper. For ESI and crystallographic data in CIF or other electronic format see DOI: 10.1039/c7ce01366c

moderately strong hydrogen bonds through both of its oxygen atoms.[16] This result suggests that, when designing new linkage isomer switches, fragments containing hydrogen bond donor groups should be avoided. This would be an unfortunate design limitation, given that hydrogen bonds are traditionally one of crystal engineering's most important and useful tools.[17] Avoiding their presence completely makes the rational design of new photo-switchable crystal systems an even more formidable task.

Here, we report two new metal–nitrite complexes that contain moderately strong intermolecular hydrogen bonds to a nitro-(η^1-NO_2) ligand. We show that the detrimental effect of these interactions on the nitro → nitrito conversion process can be mitigated by careful control of the experiment temperature, providing a positive new outlook on the compatibility of hydrogen bonds and linkage isomer switching in the solid-state.

Experimental

Synthetic procedures

$K_2[Pd(NO_2)_4]$ and $K_2[Pt(NO_2)_4]$ were synthesized following a literature procedure.[18] Et_4dien and NaOTf were used as-purchased from Sigma Aldrich and all preparations were carried out in air.

Synthesis of complex 1, [Pd(Et_4dien)(NO_2)]OTf. A solution of Et_4dien (1 mmol) in acetone (5 mL) was added to an aqueous solution of $K_2[Pd(NO_2)_4]$ (1 mmol, 2 mL). The reaction mixture was stirred at room temperature for *ca.* 3 h, before an excess of NaOTf (2 mmol) in water was added. A pale-yellow precipitate formed immediately, which was collected and dried *in vacuo*. **1** was recrystallised from a dichloromethane/diethyl ether mix.

CHN. Expected: C = 30.21%; H = 5.66%; N = 10.84%.

Found: C = 30.36%; H = 5.75%; N = 10.98%.

^{1}H NMR (500 MHz, $CDCl_3$). δ_H 1.87 (12H, t, CH_3); δ_H 2.85–2.99 (12H, m, CH_2 – overlapped); δ_H 3.44 (4H, td, CH_2).

IR. ν(N–O) = 1245, 1464 cm^{-1}; ν(N–H) = 3082 cm^{-1}.

Synthesis of complex 2, [Pt(Et_4dien)(NO_2)]OTf. A solution of Et_4dien (1 mmol) in acetone (5 mL) was added to an aqueous solution of $K_2[Pt(NO_2)_4]$ (1 mmol, 2 mL). The reaction mixture was stirred at room temperature for *ca.* 12 h, before an excess of NaOTf (2 mmol) in water was added. The solvent was removed *in vacuo*, the residue taken up in dichloromethane and then filtered to remove any inorganic salt impurities. **2** was recrystallized from a dichloromethane/diethyl ether mix.

CHN. Expected: C = 25.79%; H = 4.83%; N = 9.25%.

Found: C = 25.95%; H = 5.26%; N = 9.14%.

^{1}H NMR (500 MHz, $CDCl_3$). δ_H 1.75 (12H, t, CH_3); δ_H 2.82 (8H, m, CH_2); δ_H 2.96 (4H, m, CH_2); δ_H 3.38 (4H, td, CH_2).

IR. ν(N–O) = 1245, 1463 cm^{-1}; ν(N–H) = 3081 cm^{-1}.

Single-crystal X-ray crystallography

Single-crystal X-ray diffraction data were recorded on a Rigaku-Oxford Diffraction Gemini A Ultra diffractometer, equipped with an Atlas CCD detector and Oxford Cryosystems CryojetXL system for temperature control. Data collection, indexing and integration were performed using the Rigaku-Oxford Diffraction software CrysAlisPro. Structures were solved by dual-space methods in SHELXT,[19] and refined by full matrix least-squares on F^2 in SHELXL.[20] Hydrogen atoms were positioned geometrically and refined using a riding model. The hydrogen atom isotropic displacement parameters were fixed to U_{iso}(H) = 1.5× (for CH_3) or U_{iso}(H) = 1.2× (for CH_2 or NH) the U_{eq} of the parent atom.

In situ photocrystallography

For photocrystallographic studies, the X-ray set-up described above was modified to incorporate a purpose-built LED ring array,[21] positioning five LEDs (400 nm: Bivar UV5TZ-400-15, λ_p = 400 ± 2.5 nm, 3.4 V, 15 mA, 40 mW) at a distance of approximately 1 cm from the crystal in a uniform arc. This set-up ensures even irradiation on all sides of the crystal, and enables the collection of complete single-crystal X-ray data while the array remains in place.

Results and discussion

Complex 1: ground-state single-crystal X-ray structure

A crystal of **1** was flash-frozen at 100 K and the GS single-crystal X-ray structure was determined in the dark. **1** crystallizes in the monoclinic space group $P2_1/n$ with one Pd(II) cation and one OTf anion in the asymmetric unit. The Pd(II)-centre adopts square-planar geometry, with one tridentate Et_4dien ligand and one monodentate nitrite group occupying the coordination sphere.

The ambidentate nitrite ligand adopts solely the nitro-(η^1-NO_2) geometry in the flash-cooled GS. Fig. 1a shows the full atomic connectivity in the asymmetric unit, and Table 1 gives selected single-crystal X-ray data for the GS structure of **1**.

Fig. 1b shows the GS packing arrangement. 1-D chains of Pd-cations extend parallel to the *b*-axis, formed by discrete $D_1^1(2)$ hydrogen bonds linking the 2° amine donor group N(3)–H(3) on one molecule to the nitro O(1) acceptor on the next, symmetry-related cation (Fig. 1c). This hydrogen bond motif is significant, as it directly involves the potentially photo-active nitro-(η^1-NO_2) groups. The hydrogen bonds must be disrupted for photo-isomerisation to proceed and, given the literature precedent,[16] could be likely to hinder high photo-conversion in **1**. The OTf anions sit in discrete pockets, with each OTf participating in short contacts with 6 nearest neighbour cations. These contacts are primarily weak C–H···O or C–H···F interactions between OTf and neighbouring Et_4dien ligands, and are unlikely to strongly influence any potential photo-isomerisation.

Complex 1: steady-state photocrystallography

Steady-state studies with 1 at 100 K. The same crystal of **1** was held at 100 K and irradiated *in situ* with 400 nm LED light, using the set-up outlined above. After 1 h, the LEDs

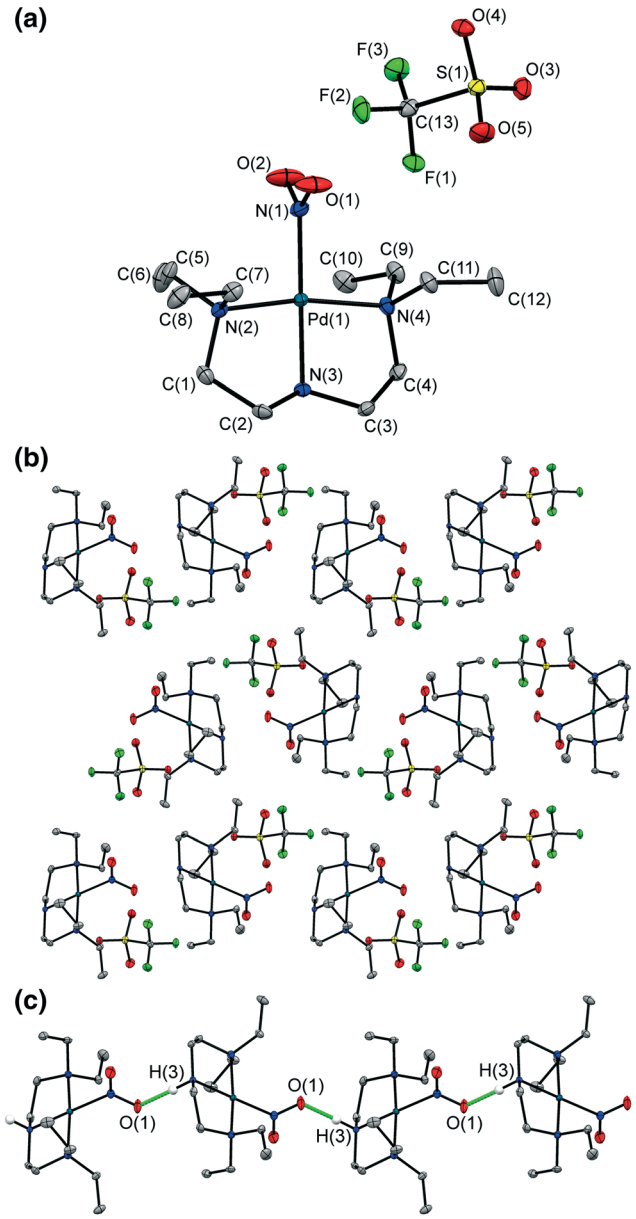

Fig. 1 (a) Atomic connectivity in the GS structure of **1**, ellipsoids at 50% probability and hydrogen atoms removed for clarity. (b) Packing diagram for the GS of **1** at 100 K, viewed along the *a*-axis, *b*-axis horizontal. (c) 1D hydrogen bonded chains of cations in **1**, extending parallel to the *b*-axis.

were switched off and a second X-ray dataset was recorded. This MS structure contains a mixture of nitrite arrangements. 44% of the structure remains as the GS nitro-(η^1-NO_2) form, while 29% has converted to an *endo*-nitrito-(η^1-ONO) isomer (Fig. 2a). Unusually, the remaining 27% of the crystal is found to adopt *exo*-nitrito-(η^1-ONO) geometry (Fig. 2b). The *exo*-ONO isomer is often formed when metal–nitrito species are intentionally prepared under certain crystallization conditions,[22,23] but is only rarely observed, at low occupancy, as a result of irradiation. As such, this result is of interest. Further irradiation caused no appreciable change in the linkage isomer ratios, indicating that a photostationary state had been achieved in **1** at 100 K.

There is a unit cell volume decrease of $\Delta V = -35.6(1)$ Å^3 (or −1.75% of the GS cell) on irradiation of **1** at 100 K, which is statistically significant.[24] This is in contrast to the majority of photo-switchable nitrite linkage isomers reported, which more typically show an expansion of the crystal on activation.[6–8] The unit cell reduction is anisotropic: while the *b* and *c* axes contract by −0.1256(5) Å and −0.230(1) Å respectively, the *a*-axis lengthens by 0.0867(5) Å. Given that the 1-D chains of metal cations extend parallel to the *a*-axis, it might be argued that the expansion in this direction is a direct result of the isomerisation. However, the overall decrease in unit cell volume would suggest that the photo-induced nitrito isomers occupy less overall volume than the GS nitro-(η^1-NO_2) form. This observation can be quantitatively confirmed by comparing the Hirshfeld surface volume for the cation molecules in each of the GS and MS structures (see section 1 in the ESI†).[25]

The hydrogen bond network in the GS of **1** must be broken for photo-excitation to occur and, following activation, neither of the photo-induced nitrito isomers form significant hydrogen bonds in the MS. This provides a possible explanation for the incomplete photo-conversion achieved at 100 K. It appears that irradiation is insufficient to break all of the hydrogen bonds required for complete photo-excitation, which again indicates that strong intermolecular interactions are detrimental for photo-induced linkage isomer conversion in the single-crystal.

The crystal held in its photostationary state was next subject to variable temperature parametric studies, to ascertain the behaviour of the photo-active isomers with temperature. The crystal was warmed in 10 K steps and an X-ray dataset obtained at each interval to reveal the nitrite isomer ratio. The results of these studies are given in Table 2. Between 100 and 120 K, while the GS isomer occupancy remains constant, within error, the *exo*-ONO occupancy is found to decrease, with a concomitant increase in *endo*-ONO. This suggests that the *exo*-ONO isomer, while sufficiently metastable to be observed at very low temperature, decays directly into the *endo*-ONO geometry with only a small thermal energy barrier. As such, the relative nitrite isomer stability in **1** at 100 K is *exo*-nitrito-(η^1-ONO) < *endo*-nitrito-(η^1-ONO) < nitro-(η^1-NO_2).

Steady-state studies with 1 at 150 K. On observing that the *endo*-ONO isomer remains metastable at 150 K, it was apparent that a second steady-state investigation was required at this temperature, to see if a different photo-response could be achieved above the metastable limit of the *exo*-ONO form. The same crystal of **1** was warmed to room temperature, clearing any residual ES, then flash-frozen to 150 K. As a reference, a 150 K GS was first obtained. The GS structures at 150 and 100 K are near-identical, excepting an expected volume increase with temperature (Table 1). The nitrite ligand adopts nitro-(η^1-NO_2) geometry and still forms 1-D hydrogen bond chains (Fig. 1c).

Table 1 Selected single-crystal X-ray data for **1** in the ground-state, GS, (before irradiation) and metastable state, MS, (after irradiation) at 100 and 150 K

	GS (100 K)	MS (100 K)	GS (150 K)	MS (150 K)
Photo-conversion	0%	56% (29% *endo*, 27% *exo*)	0%	100% (100% *endo*)
Temperature	100 K	100 K	150 K	150 K
Wavelength	0.71073 Å	0.71073 Å	0.71073 Å	0.71073 Å
Empirical formula	$C_{13}H_{29}F_3N_4O_5Pd_1S_1$	$C_{13}H_{29}F_3N_4O_5Pd_1S_1$	$C_{13}H_{29}F_3N_4O_5Pd_1S_1$	$C_{13}H_{29}F_3N_4O_5Pd_1S_1$
Formula weight	516.86	516.86	516.86	516.86
Crystal size	0.45 × 0.24 × 0.20	0.45 × 0.24 × 0.20	0.45 × 0.24 × 0.20	0.45 × 0.24 × 0.20
Crystal system	Monoclinic	Monoclinic	Monoclinic	Monoclinic
Space group	$P2_1/n$	$P2_1/n$	$P2_1/n$	$P2_1/n$
Unit cell parameters (constrained)	a = 9.2030(3) Å	a = 9.2897(4) Å	a = 9.2318(4) Å	a = 9.2793(5) Å
	b = 13.1728(5) Å	b = 13.0472(5) Å	b = 13.1472(6) Å	b = 12.9527(7) Å
	c = 16.9033(6) Å	c = 16.6730(8) Å	c = 17.0207(9) Å	c = 16.6542(10) Å
	β = 97.388(4)°	β = 98.853(4)°	β = 96.736(5)°	β = 99.379(4)°
Volume	2032.4(1) Å^3	1996.8(2) Å^3	2051.6(2) Å^3	1974.9(2) Å^3
Z	4	4	4	4
Density (calculated)	1.689 Mg m^{-3}	1.721 Mg m^{-3}	1.673 Mg m^{-3}	1.738 Mg m^{-3}
Absorption coefficient μ	1.074 mm^{-1}	1.093 mm^{-1}	1.064 mm^{-1}	1.105 mm^{-1}
F(000)	1056	1056	1056	1056
$R_{(int)}$	0.0360	0.0285	0.0301	0.0306
Completeness (to θ = 25.00°)	0.997	0.995	0.997	0.995
R_1 (observed data: $I > 2\sigma(I)$)	0.0284	0.0313	0.0309	0.0323
wR_2 (all data)	0.0603	0.0697	0.0649	0.0668
Reflections (independent)	9352(4145)	8848(4068)	9030(4196)	8451(4028)

The crystal was held at 150 K and irradiated with 400 nm LED light. After 1 h the LEDs were switched off and the MS structure determined at 150 K. In contrast to results at 100 K, irradiation at 150 K induces 100% conversion to the *endo*-ONO form (Fig. 2a), with no evidence of an *exo*-ONO isomer. The unit cell volume again decreases, with ΔV = −76.7(2) Å^3 (or −3.74% of the GS unit cell). The GS hydrogen bond network is now entirely disrupted to enable complete photo-conversion, and the MS *endo*-ONO structure shows no significant hydrogen bonding to neighbouring molecules.

Finally, variable temperature parametric studies conducted at 150–300 K determine the temperature range over which the *endo*-ONO isomer is metastable (Table 3). The crystal regains GS nitro geometry by 190 K, indicating the MS limit region in **1**.

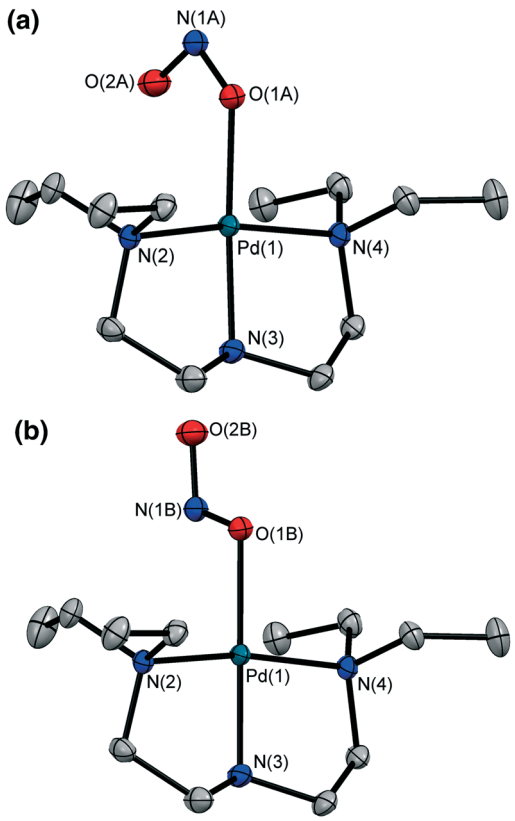

Fig. 2 Metastable state linkage isomer geometries for the cation in **1**, from single crystal X-ray structures at 100 K, (a) *endo*-nitrito-(η^1-ONO) isomer, (b) *exo*-nitrito-(η^1-ONO) isomer. Ellipsoids at 50% probability and hydrogen atoms removed for clarity.

Complex 2: ground-state single-crystal X-ray structure

A crystal of **2** was flash-frozen at 100 K and a GS X-ray structure determined in the dark. **2** is both isomorphous and isostructural with **1** and, excepting the exchange of Pd(II) for

Table 2 Nitro : nitrito isomer occupancy ratios, refined from single-crystal X-ray data in steady-state photocrystallography studies with **1** at 100 K

Temp/K	Irradiation time/h	Nitrite occupancy level		
		Nitro	*endo*-Nitrito	*exo*-Nitrito
100	0	1.00	0.00	0.00
100	1	0.44	0.28	0.27
100	2	0.44	0.28	0.27
110	2	0.43	0.40	0.17
120	2	0.43	0.57	0.00
130	2	0.43	0.57	0.00
140	2	0.43	0.57	0.00
150	2	0.44	0.56	0.00

Table 3 Nitro : nitrito isomer occupancy ratios refined from single-crystal X-ray data in steady-state photocrystallography studies with **1** at 150 K

Temp/K	Irradiation time/h	Nitrite occupancy level		
		Nitro	*endo*-Nitrito	*exo*-Nitrito
150	0	1.00	0.00	0.00
150	1	0.00	1.00	0.00
170	1	0.05	0.95	0.00
180	1	0.37	0.63	0.00
190	1	1.00	0.00	0.00
210	1	1.00	0.00	0.00
250	1	1.00	0.00	0.00
300	1	1.00	0.00	0.00

Table 5 Nitro : nitrito isomer occupancy ratios, refined from single-crystal X-ray data in steady-state photocrystallography studies with **2** at 100 K

Temp/K	Irradiation time/h	Nitrite occupancy level		
		Nitro	*endo*-Nitrito	*exo*-Nitrito
100	0	1.00	0.00	0.00
100	1	0.71	0.22	0.07
100	2	0.40	0.50	0.10
100	3	0.32	0.56	0.12
110	3	0.32	0.57	0.10
120	3	0.32	0.62	0.05
130	3	0.33	0.63	0.04
140	3	0.34	0.66	0.00
150	3	0.33	0.67	0.00

Pt(II), its GS structure is otherwise well described by Fig. 1 (see also Fig. S2†). Table 4 shows selected X-ray data for the 100 K GS of **2**.

Complex 2: steady-state photocrystallography

Steady-state studies with 2 at 100 K. The same single-crystal of **2** was held at 100 K and irradiated *in situ* with 400 nm LED light. As in the 100 K MS of **1**, this experiment confirmed that irradiation of **2** at 100 K produces a mixture of linkage isomers.

After 1 h irradiation, an X-ray dataset revealed that 22% of the crystal was converted to a MS *endo*-ONO isomer, 7% to *exo*-ONO, with the remaining 71% in GS NO_2 geometry (Fig. S3†). Further irradiation increased the ES isomer occupancy levels, with a photostationary state of 32% NO_2, 56% *endo*-ONO and 12% *exo*-ONO isomers achieved after a total of 3 h illumination. Analysis of the Hirshfeld surface volume for the cation in the GS and MS structures of **2** confirm that, as for **1**, the photo-isomers occupy less volume than the GS NO_2 form (Fig. S4 and Table S2†).

Variable temperature parametric studies next followed the variation in the nitro : nitrito occupancies on warming. Table 5 confirms that *exo*-ONO is observed between 100 and 130 K, however, as for the 100 K MS of **1**, this isomer gradually decays into the *endo*-ONO geometry across this temperature range.

Steady-state studies with 2 at 200 K. Preliminary temperature scans with **2** indicated that MS isomers remain present above 200 K, therefore a second steady-state photocrystallographic experiment was conducted at this temperature. A similar crystal was flash-cooled to 200 K and a GS X-ray structure obtained, which again compared well to the GS at 100 K (Table 4).

The crystal was held at 200 K and irradiated *in situ* with 400 nm LED light. The results of these studies are given in Table 6. A photostationary state of 93% *endo*-ONO and 7%

Table 4 Selected single-crystal X-ray data for **2** in the ground-state, GS, (before irradiation) and metastable state, MS, (after irradiation) at 100 and 200 K

	GS	MS	GS	MS
Photo-conversion	0%	68% (56% *endo*, 12% *exo*)	0%	93% (93% *endo*)
Temperature	100 K	100 K	200 K	200 K
Wavelength	0.71073 Å	0.71073 Å	0.71073 Å	0.71073 Å
Empirical formula	$C_{13}H_{29}F_3N_4O_5Pt_1S_1$	$C_{13}H_{29}F_3N_4O_5Pt_1S_1$	$C_{13}H_{29}F_3N_4O_5Pt_1S_1$	$C_{13}H_{29}F_3N_4O_5Pt_1S_1$
Formula weight	605.55	605.55	605.55	605.55
Crystal size	0.50 × 0.26 × 0.07	0.50 × 0.26 × 0.07	0.49 × 0.21 × 0.09	0.49 × 0.21 × 0.09
Crystal system	Monoclinic	Monoclinic	Monoclinic	Monoclinic
Space group	$P2_1/n$	$P2_1/n$	$P2_1/n$	$P2_1/n$
Unit cell parameters (constrained)	a = 9.2331(3) Å	a = 9.3067(4) Å	a = 9.2636(3) Å	a = 9.3268(2) Å
	b = 13.1391(4) Å	b = 13.0046(5) Å	b = 13.1409(4) Å	b = 12.9755(3) Å
	c = 16.9695(5) Å	c = 16.7285(8) Å	c = 17.1074(6) Å	c = 16.7508(4) Å
	β = 97.100(3)°	β = 99.001(4)°	β = 96.567(3)°	β = 99.170(2)°
Volume	2042.9(1) Å^3	1999.7(2)	2068.9(1) Å^3	2001.3(1)
Z	4	4	4	4
Density (calculated)	1.969 Mg m^{-3}	2.011 Mg m^{-3}	1.944 Mg m^{-3}	2.010 Mg m^{-3}
Absorption coefficient μ	7.028 mm^{-1}	7.180 mm^{-1}	6.940 mm^{-1}	7.174 mm^{-1}
F(000)	1184	1184	1184	1184
$R_{(int)}$	0.0267	0.0355	0.0399	0.0388
Completeness (to θ = 25.00°)	0.998	0.997	0.997	0.998
R_1 (observed data: $I > 2\sigma(I)$)	0.0279	0.0358	0.0213	0.0187
wR_2 (all data)	0.0666	0.0854	0.0487	0.0429
Reflections (independent)	10 322(4173)	9264(4085)	17 464(4226)	21 907(4086)

Table 6 Nitro : nitrito isomer occupancy ratios, refined from single-crystal X-ray data in steady-state photocrystallography studies with **2** at 150 K

Temp/K	Irradiation time/h	Nitrite occupancy level		
		Nitro	*endo*-Nitrito	*exo*-Nitrito
200	0	1.00	0.00	0.00
200	1	0.11	0.89	0.00
200	2	0.08	0.92	0.00
200	3	0.07	0.93	0.00
210	3	0.08	0.92	0.00
220	3	0.09	0.91	0.00
230	3	0.18	0.82	0.00
240	3	0.66	0.34	0.00
250	3	1.00	0.00	0.00
300	3	1.00	0.00	0.00

GS nitro NO_2 isomers was achieved after 3 h irradiation, which is – to the author's knowledge – the highest-reported photo-conversion in a Pt(II) linkage isomer to-date. Similarly to **1**, no evidence of the *exo*-ONO form was found at this higher temperature. Variable temperature parametric studies show that the MS limit for the photo-induced *endo*-ONO isomer in **2** lies in the region of 230–240 K, with the crystal returning to its GS NO_2 isomer by 250 K.

Comparison of photo-isomerisation behaviour at low *vs.* higher temperature in 1 and 2

The dramatic contrast in the photo-response of **1** and **2** at low *vs.* higher temperatures indicates that one or more factors influencing isomerisation are strongly temperature-dependent.

The first contrast is the fact that the *exo*-ONO isomer is only present in the MS structures obtained at 100 K. Previous reports of photo-induced *exo*-ONO isomers suggest that this species is an intermediate existing in the pathway between GS NO_2 and MS *endo*-ONO forms.[5] The present results support this theory, as *exo*-ONO decays directly into *endo*-ONO on warming with no change in GS NO_2 occupancy. Despite this, the fact that the *exo*-ONO occupancy is as high as 27% for **1** and 12% for **2**, even after the light is removed, does suggest that the *exo*-ONO isomer is an independent ES with its own stability range. The *exo*-ONO isomer has decayed by 120 K in **1** and by 140 K in **2**, which indicates that its ES lifetime is too short to be observed by steady-state photocrystallographic methods above these temperatures.[26] This would explain why there is no evidence of the *exo*-ONO form at 150 or 200 K.

It is also interesting to compare the overall photo-activation level in **1** and **2** at each temperature. Despite the presence of multiple MS isomers at 100 K, excitation remains incomplete: for **1** the combined *exo*- and *endo*-ONO ratios give an overall conversion of 56%, in **2** the sum is 68%. In contrast, much higher photo-conversion is achieved in **1** and **2** at higher temperature, with 100% excitation in **1** after just 1 h at 150 K.

There are several structural factors that may explain these observations. Firstly, we reflect that all of the structures contain hydrogen bonding to the GS NO_2 group. In the GS structures of **1** and **2**, the $NO_2\cdots$amine interaction is linear and a comparison of the hydrogen bond distances is given in Tables 7 and 8. In line with thermal lattice expansion, the N(3)–H(3)···O(1) hydrogen bonds are significantly longer at higher temperature, consistent with these interactions becoming weaker on warming. If, as expected, hydrogen bonds to the GS NO_2 ligand inhibit photo-isomerism,[16] the weaker interaction at high temperature is expected to facilitate higher conversion. Secondly, it has been previously shown that "reaction cavity" analysis – where a reaction cavity is defined as the volume encapsulating the photo-active group – provides insight into local structural changes and helps to rationalize how or why a photo-reaction proceeds.[14,15] Tables 9 and 10 (and Fig. S5 and S6†) show reaction cavity analyses for the GS and MS structures of **1** and **2**. For both complexes, the GS reaction cavity volumes are larger at higher temperatures. This indicates that there is more available space, and so fewer steric restrictions, in the vicinity of the NO_2 ligand at higher temperatures, which may help the reaction to proceed to higher conversion. In addition, the overall change in reaction cavity volume on photo-activation (ΔV_c) can be used to provide a measure of how much the local structure must change in order to accommodate linkage isomer photo-switching. For a single-crystal-to-single-crystal transformation, we expect that the reaction proceeding with the least amount of movement or structural rearrangement will impart the least strain to the surrounding crystalline array, and will therefore be most favourable.[28] As such, we expect that the reaction requiring the smallest change in the vicinity of the photo-switching nitrite ligand (*i.e.* smallest ΔV_c) will lead to highest photo-conversion. For **1**, ΔV_c is ~3.4× smaller at 150 K than 100 K, while for **2** ΔV_c is ~1.8× smaller at 200 K than 100 K. This provides a rationale for why higher conversion levels can be accommodated at higher temperatures in both of the complexes.

Comparison of photo-isomerisation behaviour in 1 and 2

Under steady-state photocrystallographic conditions, the isomerisation behaviour in the isostructural crystals of **1** and **2**

Table 7 N(3)–H(3)···O(1) hydrogen bonding interactions in the GS structures of **1** and 100 K and 150 K

Temp/K	Graph set	Symmetry operation	D···A distance/Å
100	$D_1^1(2)$	$\frac{1}{2}-x, -\frac{1}{2}+y, \frac{1}{2}-z$	2.801(3)
150	$D_1^1(2)$	$\frac{1}{2}-x, -\frac{1}{2}+y, \frac{1}{2}-z$	2.815(3)

Table 8 N(3)–H(3)···O(1) hydrogen bonding interactions in the GS structures of **2** and 100 K and 200 K

Temp/K	Graph set	Symmetry operation	D···A distance/Å
100	$D_1^1(2)$	$\frac{1}{2}-x, -\frac{1}{2}+y, \frac{1}{2}-z$	2.798(6)
200	$D_1^1(2)$	$\frac{1}{2}-x, -\frac{1}{2}+y, \frac{1}{2}-z$	2.810(4)

Table 9 Reaction cavity (V_c) analysis for GS and MS of **1** at 100 and 150 K. V_c determined by removing the nitrite group and performing a contact surface void space calculation in Mercury[27] (probe radius 1.2 Å, grid spacing 0.1 Å)

	Temp/K	V_c per unit cell/Å^3	V_c per molecule/Å^3	ΔV_c (MS–GS)/%
GS	100	127.66	31.92	
MS	100	139.04	34.76	8.91
GS	150	133.05	33.26	
MS	150	136.51	34.13	2.60

Table 10 Reaction cavity (V_c) analysis for GS and MS of **2** at 100 and 200 K. V_c determined by removing the nitrite group and performing a contact surface void space calculation in Mercury[27] (probe radius 1.2 Å, grid spacing 0.1 Å)

	Temp/K	V_c per unit cell/Å^3	V_c per molecule/Å^3	ΔV_c (MS–GS)/%
GS	100	132.30	33.08	
MS	100	138.02	34.51	4.32
GS	200	138.23	34.56	
MS	200	141.53	35.38	2.37

is generally very similar, indicating that the primary factor controlling linkage isomer photo-switching in these materials is the surrounding crystal structure. However, there are two key differences in the photo-responses of **1** and **2** that should be considered. The first is that the photo-reaction rate is much slower for the Pt-cation in **2** than for the Pd system **1**. There is precedent for slower reaction kinetics in photo-active linkage isomer crystals with heavier transition metals (TMs),[29] and this has generally been linked to the expectation of lower kinetic lability for ligands attached to heavier TMs.[30] Secondly, though high photo-activation is achieved in both **1** and **2** at 150 and 200 K respectively, despite structural similarities 100% conversion is only reached in the Pd-system **1**. Alongside similar arguments for the relative kinetic lability of the nitrite ligand in each complex, this slight discrepancy in excitation level could also be attributed to their absorption profiles (Fig. S7†). There is a blue shift in the absorption spectrum of **2** compared with **1**, suggesting that lower excitation wavelengths could improve conversion. However, test studies at wavelengths between 365 and 395 nm could not induce 100% photo-excitation in **2**, and instead led to crystal degradation.

Conclusions

The results of this, and previous,[16] photocrystallographic studies confirm that intermolecular hydrogen bonding involving the photo-active group will influence the progress of nitro → nitrito conversion in the solid-state. However, in contrast to previous work, this study has illustrated that the presence of such intermolecular interactions does not necessarily limit the crystal system to only a low photo-activation level. Careful control of the experiment temperature not only influences the ES lifetime,[5,31] but can also be used to control the maximum level of excitation in hydrogen bonded systems. There has been a prior assumption that, for each crystal system, there is a fixed overall level of achievable MS occupation, bound either by the steric properties of the crystal or the electronic properties of the active molecule.[4,8,32,33] This study challenges that supposition, and the observation of temperature-regulated photo-activation adds a new dimension of control for single-crystal-to-single-crystal linkage isomer transformations, which may be exploited in future device technologies. Importantly, in terms of crystal engineering, the inclusion of hydrogen bond donor groups need not be avoided, a factor that will assist in the targeted design of new linkage isomer systems aimed towards specific photo-switching applications.

Conflicts of interest

There are no conflicts to declare.

Acknowledgements

The authors would like to that the UK Engineering and Physical Sciences Research Council (EPSRC) for financial support. This work is supported by EPSRC Programme Grant EP/K004956/1.

Notes and references

1 A. Werner, *Ber. Dtsch. Chem. Ges.*, 1907, **40**, 765–788.
2 M. D. Carducci, M. R. Pressprich and P. Coppens, *J. Am. Chem. Soc.*, 1997, **119**, 2669–2678.
3 P. Coppens, I. Novozhilova and A. Kovalevsky, *Chem. Rev.*, 2002, **102**, 861–884.
4 B. Cormary, S. Ladeira, K. Jacob, P. G. Lacroix, T. Woike, D. Schaniel and I. Malfant, *Inorg. Chem.*, 2012, **51**, 7492–7501.
5 L. E. Hatcher, J. Christensen, M. L. Hamilton, J. Trincao, D. R. Allan, M. R. Warren, I. P. Clarke, M. Towrie, D. S. Fuertes, C. C. Wilson, C. H. Woodall and P. R. Raithby, *Chem. – Eur. J.*, 2014, **20**, 3128–3134.
6 L. E. Hatcher, M. R. Warren, D. R. Allan, S. K. Brayshaw, A. L. Johnson, S. Fuertes, S. Schiffers, A. J. Stevenson, S. J. Teat, C. H. Woodall and P. R. Raithby, *Angew. Chem., Int. Ed.*, 2011, **50**, 8371–8374.
7 M. Warren, S. Brayshaw, A. Johnson, S. Schiffers, P. Raithby, T. Easun, M. George, J. Warren and S. Teat, *Angew. Chem.*, 2009, **121**, 5821–5824.
8 L. E. Hatcher, *CrystEngComm*, 2016, **18**, 4180–4187.
9 J. M. Cole, K. Y. M. Yeung, G. Pace, S. O. Sylvester, D. Mersch and R. H. Friend, *CrystEngComm*, 2015, **17**, 5026–5031.
10 K. F. Bowes, J. M. Cole, S. L. G. Husheer, P. R. Raithby, T. L. Savarese, H. A. Sparkes, S. J. Teat and J. E. Warren, *Chem. Commun.*, 2006, 2448–2450.
11 A. Y. Kovalevsky, K. A. Bagley, J. M. Cole and P. Coppens, *Inorg. Chem.*, 2002, **42**, 140–147.
12 D. V. Fomitchev, K. A. Bagley and P. Coppens, *J. Am. Chem. Soc.*, 2000, **122**, 532–533.

13 P. Coppens, M. D. Carducci, K. Culp and D. Fomitchev, *Abstracts of Papers of the American Chemical Society*, 1997, vol. 214, p. 318.
14 Y. Ohashi, *Crystallogr. Rev.*, 2013, **19**, 2–146.
15 Y. Ohashi, *Acc. Chem. Res.*, 1988, **21**, 268–274.
16 L. E. Hatcher, E. J. Bigos, M. J. Bryant, E. M. MacCready, T. P. Robinson, L. K. Saunders, L. H. Thomas, C. M. Beavers, S. J. Teat, J. Christensen and P. R. Raithby, *CrystEngComm*, 2014, **16**, 8263–8271.
17 G. R. Desiraju, *Chem. Commun.*, 1997, 1475–1482.
18 R. D. Feltham, G. Elbaze, R. Ortega, C. Eck and J. Dubrawski, *Inorg. Chem.*, 1985, **24**, 1503–1510.
19 G. Sheldrick, *Acta Crystallogr., Sect. A: Found. Adv.*, 2015, **71**, 3–8.
20 G. Sheldrick, *Acta Crystallogr., Sect. C: Struct. Chem.*, 2015, **71**, 3–8.
21 S. K. Brayshaw, J. W. Knight, P. R. Raithby, T. L. Savarese, S. Schiffers, S. J. Teat, J. E. Warren and M. R. Warren, *J. Appl. Crystallogr.*, 2010, **43**, 337–340.
22 R. Wen, I. Bernal, S. S. Massoud, R. K. Thalji, D. R. Billodeaux and F. R. Fronczek, *Inorg. Chim. Acta*, 1999, **295**, 91–105.
23 D. Das, I. Rahaman Laskar, A. Ghosh, A. Mondal, K.-i. Okamoto and N. Ray Chaudhuri, *J. Chem. Soc., Dalton Trans.*, 1998, 3987–3990.
24 A. J. Blake, W. Clegg and J. M. Cole, *Crystal Structure Analysis: Principles and Practice*, Oxford University Press, 2009.
25 M. A. Spackman and J. J. McKinnon, *CrystEngComm*, 2002, **4**, 378–392.
26 L. E. Hatcher and P. R. Raithby, *Coord. Chem. Rev.*, 2014, **277–278**, 69–79.
27 C. F. Macrae, I. J. Bruno, J. A. Chisholm, P. R. Edgington, P. McCabe, E. Pidcock, L. Rodriguez-Monge, R. Taylor, J. v. d. Streek and P. A. Wood, *J. Appl. Crystallogr.*, 2008, **41**, 466–470.
28 A. Natarajan and B. R. Bhogala, in *Supramolecular Photochemistry*, John Wiley & Sons, Inc., 2011, pp. 175–228.
29 M. R. Warren, S. K. Brayshaw, L. E. Hatcher, A. L. Johnson, S. Schiffers, A. J. Warren, S. J. Teat, J. E. Warren, C. H. Woodall and P. R. Raithby, *Dalton Trans.*, 2012, **41**, 13173–13179.
30 P. Atkins, P. W. Atkins and D. F. Shriver, *Shriver & Atkins Inorganic Chemistry*, W.H. Freeman, 2006.
31 L. E. Hatcher, J. M. Skelton and P. R. Raithby, *Phys. Chem. Chem. Phys.*, 2017, under review.
32 L. E. Hatcher and P. R. Raithby, *Acta Crystallogr., Sect. C: Cryst. Struct. Commun.*, 2013, **69**, 1448–1456.
33 D. Schaniel and T. Woike, *Phys. Chem. Chem. Phys.*, 2009, **11**, 4391–4395.

